J. Phys. B: Atom. Molec. Phys. **13** (1980) 359–376. Printed in Great Britain

Total cross sections for electron scattering from N_2 and He

H J Blaauw†, R W Wagenaar, D H Barends and F J de Heer

FOM-Institute for Atomic and Molecular Physics, Kruislaan 407, Amsterdam/Wgm, The Netherlands

Received 28 December 1978, in final form 7 June 1979

Abstract. An apparatus has been constructed to measure the total cross section for electron scattering by atoms and molecules. It can be viewed as a linearisation of the Ramsauer technique, with a well defined solid angle for the analyser/collector. The effective length of the absorbing gas cell used in the transmission measurement could be determined accurately by comparing the results obtained with two cells of different length. Measurements on He and N_2 have been carried out for 15–750 eV electrons with an accuracy of 4% or better. The results are compared with existing experimental and theoretical data from other groups. The data for He link up within the experimental uncertainty with some recent theoretical calculations below the inelastic threshold and agree very well in the overlapping energy region with the recent experimental data of Kennerly and Bonham and of Kauppila *et al.*

1. Introduction

The knowledge of accurate experimental and theoretical data on electron scattering from atoms is very important to test the forward dispersion relation for electron–atom scattering originally formulated by Gerjuoy and Krall (1960, 1962). From a semi-empirical study we have already concluded that Gerjuoy's formulation has to be modified (de Heer *et al* 1976, 1977). But in order to perform an accurate quantitative analysis, reliable experimental total cross sections (TCS) and elastic differential cross sections (DCS) at small angles are needed, especially at electron impact energies between about 20 and 100 eV. Since such data were not available, we have built an apparatus to provide these data.

With regard to TCS measurements, a lot of experiments have been carried out as one can learn from the review article of Bederson and Kieffer (1971). Most of these experiments have been performed with the Ramsauer technique (1921a, b). But in the case of helium Bederson and Kieffer attached no higher reliability to the results than about 25% in the energy range up to 30 eV. At higher energies the situation was even worse. Recently, new interest in accurate TCS has arisen and this has resulted in a much more satisfactory situation. At low energies (up to 12 eV) Crompton *et al* (1967, 1970) and Milloy and Crompton (1977) have obtained accurate results with a swarm technique, whereas Kauppila *et al* (1977), Stein *et al* (1978) and Kennerly and Bonham (1978) have published new data in the low and intermediate energy ranges (i.e. $\leqslant 50$ eV).

This article deals with the TCS measurements we have performed on helium and molecular nitrogen in the energy range of 16–750 eV. In a preliminary form these

† Present address: Dienst IJkwezen, Van Swindenlab., PO Box 654, 2600 AR Delft.

0022-3700/80/020359+18$01.00

results have already been presented (Blaauw *et al* 1977), but now more emphasis will be laid upon the experimental arrangement. Section 2 deals with the apparatus, § 3 with the experimental procedure and errors involved, whereas in § 4 the present results will be given together with an updated (1978) list of experimental and theoretical data from other groups. The results for the other noble gases will be presented in a subsequent paper. The present results on helium have been used extensively within the framework of the forward dispersion relation (Blaauw 1979).

2. Apparatus

2.1. Scattering geometry

We have chosen the transmission technique because, in principle, it is by far the simplest. But it has been recognised that the use of the magnetic field as an energy selector—as in the Ramsauer technique—causes serious difficulties when one wants to calculate the influence of the spatial extent of the electron beam and of the electrons scattered into the solid angle of the detector on the measurement. Therefore we have not applied a magnetic field at all, but have 'linearised' the Ramsauer device which yields two main advantages over the Ramsauer technique:

(i) the angular resolution can be determined exactly, and

(ii) the set-up also permits differential scattering measurements.

Figure 1 is a very schematic sketch of this linear experimental arrangement. To illustrate the advantage concerning the angular resolution, it is essential to analyse the relation between the TCS and the attenuation of the beam in somewhat more detail. Basically this relation is the Lambert–Beer law

$$\sigma_{\text{tot}} = (NL)^{-1} \ln(I_0/I_c) \tag{2.1}$$

where N stands for the gas density in the absorption cell, L is the effective length of the electron path through the gas and I_0/I_c is the ratio of the beam intensity in front of and behind the absorption cell respectively. However, equation (2.1) represents the ideal case, in which the beam is infinitesimally narrow and the solid angle of the detector is zero. Of course, this situation is not feasible in practice and small angle scattering must be incorporated. In the same way as equation (2.1) is derived, one finds

$$\ln(I_0/I_c) = NL\sigma_{\text{tot}} - N\int_0^L \mathrm{d}x \int_0^{\Delta\Omega(x)} \left(\frac{\mathrm{d}\sigma}{\mathrm{d}\Omega}\right) \mathrm{d}\Omega \tag{2.2}$$

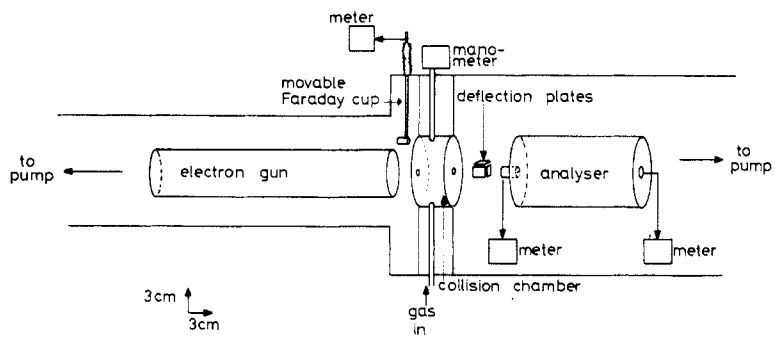

Figure 1. Schematic sketch of the apparatus.

Here $\Delta\Omega(x)$ is the solid angle of the detector as seen by a scattering event taking place at position x on the beam axis. The factor $(d\sigma/d\Omega)$ represents (depending on the kind of detector) the elastic or elastic plus inelastic DCS. To give a full quantitative account of the second term in equation (2.2), the knowledge of $(d\sigma/d\Omega)$ is necessary at small angles down to 0°. As is well known, the scattering becomes more and more forwardly peaked with increasing impact energies. For the elastic part of $(d\sigma/d\Omega)$ we can overestimate the integral expression in equation (2.2) by

$$\int_0^L dx \int_0^{\Delta\Omega(x)} \left(\frac{d\sigma}{d\Omega}\right)_{\text{elastic}} d\Omega \leqslant L\Delta\Omega\left(\frac{d\sigma}{d\Omega}\right)_{\text{elastic}} (\theta = 0°) \tag{2.3}$$

where $\Delta\Omega$ stands for the solid angle subtended by the detector entrance aperture with respect to the centre of the collision cell. $(d\sigma/d\Omega)_{\text{elastic}}$ $(\theta = 0°)$ can be found by extrapolating the available data on small angle elastic scattering from the literature. For the contribution of inelastic small angle scattering this simplification cannot be given unambiguously. At high impact energies, one is able to calculate the integral in equation (2.2) for inelastic scattering of electrons off helium with the Bethe approximation, but for the other noble gases this calculation is more complicated, in particular for excitation to the continuum states.

Firstly, to eliminate this uncertainty, we use a detector which discriminates between elastic and inelastic scattered electrons. In this case, the integral in the second term in equation (2.2) reduces to that in equation (2.3). As a second step, we choose the solid angle of the detector to be so small, that expression (2.3) can be neglected with respect to the first term in equation (2.2) far within the experimental error in σ_{tot}. In the case of helium estimations for σ_{tot} and $(d\sigma/d\Omega)_{\text{elastic}}$ $(\theta = 0°)$ are given in table 1. So when we require

$$(d\sigma/d\Omega)_{\text{elastic}}(\theta = 0°) \,.\, \Delta\Omega \leqslant 10^{-3}\sigma_{\text{tot}}$$

we conclude from the table that the second term on the right hand side of equation (2.2) is less than 0·1% compared with the first term if $\Delta\Omega \leqslant 10^{-3}$ sr. As can be seen from table 1 this requirement may be relaxed for low energies.

The scattering geometry used is indicated in figure 1. Let d_n $(n = 1, 2, 3)$ be the diameter of the entrance aperture, the exit aperture (both of the collision chamber) and the entrance aperture of the analyser respectively, let L be the length of the collision chamber and D be the distance between the centre of the collision chamber and the entrance aperture of the analyser. The following set of dimensions are chosen: $d_1 = d_2 = d_3 = 1{\cdot}0$ mm, $L = 42{\cdot}0$ mm and $D = 100{\cdot}0$ mm. The diameters d_1 and d_2 are chosen small compared to L so that possible uncertainties in the target gas density are

Table 1. Comparison of cross sections for electron–helium scattering.

E (eV)	$\left(\frac{d\sigma}{d\Omega}\right)_{\text{elastic}}$ $(\theta = 0°)$ $(a_0^2\ \text{sr}^{-1})$	Reference	σ_{tot} (a_0^2)	Reference
500	1·4	Jansen *et al* (1976)	1·4	de Heer and Jansen (1977)
200	2·3	Jansen *et al* (1976)	2·6	de Heer and Jansen (1977)
100	3·2	Jansen *et al* (1976)	4·1	de Heer and Jansen (1977)
19	2·8	Andrick and Bitsch (1975)	11·4	de Heer and Jansen (1977)
5	1·0	Andrick and Bitsch (1975)	20·1	de Heer and Jansen (1977)

localised near the orifices. Together with the diameter d_3 the requirement on the solid angle $\Delta\Omega$ is met: $\Delta\Omega = 7{\cdot}85 \times 10^{-5}$ sr.

Just in front of the analyser we placed a Faraday cup equipped with a hole in its back. The cup is 30 mm long and has a diameter of 8 mm, whereas the diameter of the hole is 1·1 mm. With the aid of deflection plates we can monitor the electron beam in this cup to achieve an optimal alignment into the analyser.

2.2. Magnetic field shielding

In order to prevent the electrons from deviating from their straight path, it is essential to shield against all present magnetic fields. Therefore:

(i) all material close to the beam is either a non-magnetic alloy of nickel and chromium, NiCr V, or molybdenum;

(ii) all stainless steel parts are selected for a low residual magnetic field, and

(iii) Helmholtz coils and double μ-metal shields are used to compensate for the Earth's magnetic field. With all these precautions we obtain an upper limit for the magnetic field on the central axis of 0·5 mG perpendicular to the axis and of 2 mG along the axis.

2.3. Vacuum system

The vacuum system has been designed in such a way, that (i) scattering takes place outside the absorption cell and (ii) scattering by other atoms or molecules than those of the target gas does not influence the signal to be measured. The collision chamber constitutes the separation between two pumping systems which are equal with regards to the construction. With oil diffusion pumps (2000 l s^{-1} at the analyser side and 700 l s^{-1} at the gun side) in this differential pumping set-up the background pressure at the analyser side was always less than 4×10^{-7} Pa and on the gun side always less than 8×10^{-7} Pa. We found a pressure drop over the exit aperture of the collision chamber of about 5000. The target gas pressure is measured with an MKS baratron 145 BHS-1. It is a membrane manometer with an internal reference vacuum. We admit the target gas to the collision chamber through an adjustable needle valve. The gas inlet system, as well as the gun and analyser are bakable to about 150 °C. Particular care was taken to prevent contamination of the gas inlet system; only if no change in the background mass spectrum was observed when admitting helium to the system, could we perform measurements.

2.4. Electron optics

To justify the application of equation (2.1) it is further necessary to shoot a narrow beam with a divergence smaller than 10^{-2} rad through the absorption cell in order to fall within the analyser aperture. We require that the beam diameter is about half the diameter of the diaphragms in the collision chamber and the analyser entrance.

2.4.1. Electron gun design. Generally, an optical system can be specified by the way the entrance window and pupil are imaged, which is governed by the law of Helmholtz–Lagrange in the case of paraxial rays. The exit pupil and window fix the diameter and divergence of the beam in the target space. In our case, where we require a parallel beam flow between collision cell and analyser, the electron gun has been designed in

such a way that its entrance pupil is imaged in the centre of the collision cell and its entrance window in the analyser aperture, both with a diameter of 0·5 mm.

It is essential that electrons with large radial velocity components are removed from the beam for two reasons: (*a*) to fulfil the requirement on the divergence of the final beam and (*b*) to keep chromatic aberrations small at low beam energies. Therefore we chose an electron gun concept developed by Harting and Burrows (1970) using a Pierce extraction system. We applied the same principles for the angle selection of the emitted electrons from the cathode surface as Harting and Burrows, but used a three cylinder zoom lens instead of a set of two cylinder lenses for moulding the final beam. For a detailed quantitative description of the electron optical system used, we refer to Blaauw (1979).

Figure 2 shows the gun with additional lenses and the potentials applied are given in table 2 for the two impact energy ranges. All the lens data used in the design are from the tables of Harting and Read (1976). We maintain their convention that D indicates the diameter of the apertures or cylinders, G the gap width between the cylinders and A the distance between the apertures or the centre of the gaps. The Pierce extraction system and the field-free region just behind the anode (1 and 2 in figure 2) act as a negative lens (lens 1) with the important property that the electrons having trajectories with the same angle with respect to the optical axis at the anode aperture originate from a virtual ring-shaped object in the focal plane of this lens. With the aid of a three aperture lens 2 ($D = 3$ mm, $A = 3$ mm) this object is projected on a very small diaphragm, the so-called stripper ($D = 0{\cdot}05$ mm) with magnification 6·0. In this way electrons which are transmitted through the stripper are angle selected. Lens 2 is used in the Einzel lens mode with the voltage ratio 1 : 2·8 : 1 (or 1 : 0·24 : 1) with respect to the anode potential. The image of the anode aperture lies 26·3 mm in front of the lens with magnification 2·4.

This anode image and the stripper can be recognised as the entrance window and pupil respectively with regard to the lens configuration behind the stripper. The

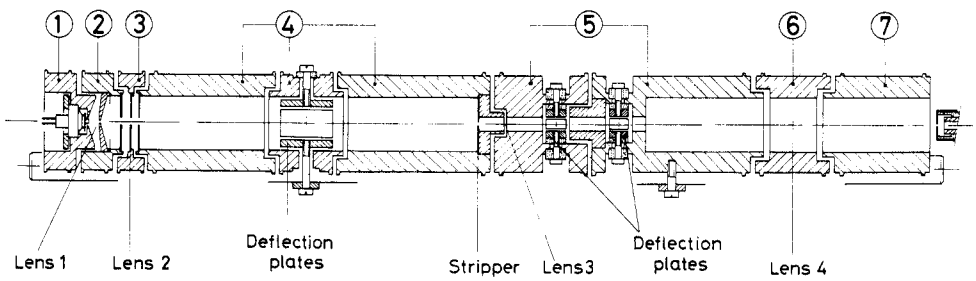

Figure 2. Vertical cross section of the electron gun (diaphragms are not to scale). The numbers refer to the electrode elements mentioned in table 2.

Table 2. List of applied voltages to the gun with respect to the cathode.

	Number of the electrodes						
Case	1	2	3	4	5	6	7
a	0	250	700	250	42	to be adjusted†	$15 \leqslant V' \leqslant 300$
b	0	250	950	950	160	to be adjusted†	$100 \leqslant V' \leqslant 1000$

† According to the tables of Harting and Read (1976).

electrons emerging from the stripper have to be brought to the proper final beam energy. We have to consider two modes of operation for the next energy regions: (*a*) between 15 and 250 eV and (*b*) above 250 eV. To keep the divergence of the beam small at the anode region, the cathode–anode spacing must not be too small (in our case 4 mm) and a rather large anode voltage (see table 2) is therefore necessary to provide a sufficient extraction field. This means that the electrons have to be strongly decelerated behind the stripper for low impact energies. To avoid the use of a very thick lens and thereby aberrations, the deceleration is done in two steps, firstly by a two cylinder lens—lens 3 ($D = 5$, $G = 0{\cdot}5$ mm)—with a voltage ratio of 6 : 1, and secondly by a three cylinder lens—lens 4 ($D = A = 20$ mm, $G = 2$ mm). Lens 4 is used as a zoom lens resulting in a fixed position of the anode image in the analyser aperture. Lens 3 is placed 10 mm behind the stripper so that the stripper is located in the first focal plane in order to keep the angles of the electron trajectories within manageable limits. In its turn, lens 4 images the stripper in its second focal plane. This focal plane shifts only 10–15 mm in the collision cell as one adjusts the middle voltage of the zoom lens in order to keep the anode image fixed at the wide range of impact energies for case (*a*) and (*b*). Another nice property of this zoom lens is that the magnification of the anode image varies only slightly for the range of potentials we apply. These two features guarantee that the conditions imposed on the final beam are fulfilled. Finally, to attain energies as high as 850 eV, we change the Einzel lens mode of lens 2 into a two aperture lens mode with a voltage ratio of 1 : 3·8.

2.4.2. Electron analyser design. The electrons are detected in a simple retarding field analyser, which is shown in figure 3. Kessler and Lindner (1964) developed the principles on which this analyser type is based, which can be applied if the transverse energy of the incoming electrons is very small compared with their total kinetic energy. The analyser is in fact a reversed version of the Soa extraction system (1959). The unscattered beam is decelerated to (almost) zero potential and passes through a small aperture (diameter 2 mm) in the retarding plate. After this retarding plate the same Soa system restores the beam energy to its original value and a three cylinder lens behind the

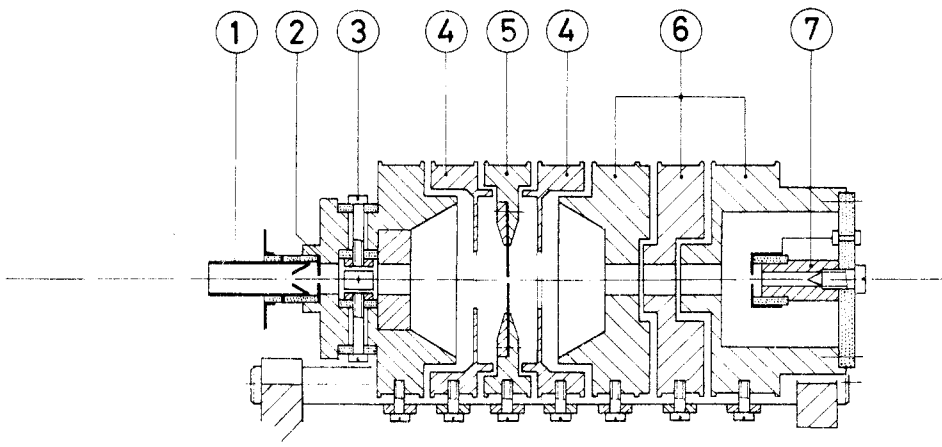

Figure 3. Vertical cross section of the retarding field analyser. 1, Faraday cup used to monitor the beam; 2, entrance aperture of the analyser; 3, deflection plates; 4, middle element of the Soa system; 5, retarding plate; 6, lens to focus the beam into 7; 7, Faraday cup.

filter lens focuses the beam with a fixed energy in the Faraday cup mounted at the back of the analyser. The energy resolution depends on the size of the entrance aperture, which in our case amounts to 0·05%: this is sufficient to separate electrons with a kinetic energy difference of 0·5 eV in the case of 1000 eV primary electrons.

2.4.3. Operation. The primary beam intensity is measured by means of a movable Faraday cup just in front of the collision chamber; this enables one to monitor for variations in the emission characteristics, which, when unnoticed, can lead to serious errors in the measured beam attenuation.

For proper operation of the optics a good alignment is needed. To correct for small mechanical misalignments several sets of deflection plates are placed in the gun and analyser, as can be seen from figures 2 and 3.

Between 25 and 850 eV we found a 100% transmission into the Faraday cup at the back of the analyser, although the diameter of the final beam was somewhat larger than expected from the applied lens data. However, the increasing magnification of the anode image with decreasing energy, together with the large spherical aberration coefficient of the Einzel lens (lens 2) cause the beam to blow up below 25 eV. In that case we used the Faraday cup in front of the analyser as a detector. This Faraday cup subtends a solid angle of $1{\cdot}03 \times 10^{-2}$ sr, so in order to apply the Lambert–Beer law, the use of this cup as a detector is only permitted below 30 eV impact energy (see table 1).

The energy spread of the beam electrons due to the thermionic emission can be measured by varying the retarding field in the analyser. Assuming the energy resolution to be 0·05% we found a full width at half maximum of the signal in the Faraday cup at the back of the analyser of 0·4 eV.

3. Experimental procedure and error discussion

3.1. Experimental procedure

The experimental procedure is based on the relation between the current attenuation and the TCS as given by equation (2.1). The procedure to measure the attenuation is as follows: firstly, the electron optics are optimally adjusted, secondly, the current I_c in the retarding field analyser is measured with the Faraday cup in front of the collision chamber in the upper position, and thirdly, this Faraday cup is moved to its lower position to intercept and measure the primary beam I_0. The TCS is then derived by comparing the ratio (I_c/I_0) with and without gas in the collision chamber according to:

$$(I_c/I_0)_{gas}/(I_c/I_0)_{vac} = \exp(-NL\sigma_{tot}). \tag{3.1}$$

In this way we do not need to take into account the collection efficiencies of the Faraday cups. Besides, the error due to a non-optimal calibration of the meters with which the Faraday cup signals are measured is eliminated; only their linearity is important.

For the typical pressures we apply (less than 5 Pa) it is legitimate to consider the gas as an ideal gas, which permits a direct relation between the density N and the gas pressure in the collision chamber. The baratron sensing head with which this pressure is measured, is kept at the elevated temperature of 322 K, a facility supplied by the manufacturer to protect the membrane housing against thermal fluctuations. This means however, that by thermal transpiration there exists a small pressure drop over the tube which connects the baratron with the collision chamber at low pressures.

It has been generally accepted that, if the mean free path length of the gas molecules is much larger than the diameter of the orifice or tube connection between the region at high (T_h) and low (T_c) temperature, the relation is valid as formulated by Knudsen (1910) for this pressure drop:

$$R \equiv (P_c/P_h) = (T_c/T_h)^{1/2}. \tag{3.2}$$

At higher pressures, where the mean free path length becomes much smaller than the specific dimensions of the apparatus, the collisions between the molecules themselves dominate, which results in the disappearance of the pressure drop. So, there exists a so-called 'transition region' where the value of R as given by equation (3.2) reaches unity asymptotically with increasing pressure.

Indeed at low pressures, Edmonds and Hobson (1965) measured the thermal transpiration ratio, as given by the Knudsen formula, in the case of an orifice as connecting element, but for tube connections their measured value of R was higher. This particular value appeared to be dependent on the tube diameter and the exact location of the temperature transition along the tube, but not significantly on the specific target gas. However, they were not able to formulate an analytical expression for R as a function of pressure and tube diameter, without prior knowledge of the low pressure limit for R.

Bromberg (1969) was the first who measured R for a capacitance manometer—with a McLeod gauge as a calibrating instrument—and found a value of 0·99 instead of 0·96 according to equation (3.2).

Three years later Baldwin and Gaerttner (1973) did the same, but found 0·974 for R as the low pressure limit, significantly lower than Bromberg but still higher than the Knudsen limit. The discrepancy between their results can be ascribed to the difference in diameter of the connecting tubes (12·7 mm for Bromberg and 3·15 mm for Baldwin and Gaerttner).

This short review leads us to the conclusion that there is no agreement about the magnitude of the effect. The most obvious way for us to get out of the problem was to measure the effect in our apparatus itself. We performed this following the procedure followed by Baldwin and Gaerttner, which consisted of connecting a second baratron, symmetrically with respect to the first, with the collision chamber and comparing their readings when one is at room temperature (in our case 294 K) and the other at the elevated temperature of 322 K. The tube connections were 4 mm internal diameter and about 20 cm long. The target gases used were helium, neon and krypton. Figure 4 shows the results for R as a function of the pressure. From this figure we see that the 'onset' of the transition region lies for all the three gases above 2 Pa. The low pressure limit values of R are significantly higher in comparison with what is to be expected from equation (3.2). The value of $0{\cdot}980 \pm 0{\cdot}002$ we measured lies about halfway between the value of Baldwin and Gaerttner (0·974) and that of Bromberg (0·990). From the inaccuracy of 0·3% for the low pressure data it is not legitimate to consider the differences in R between the different gases as real.

For the calculation of the actual pressure P_c in the collision chamber from the reading of the baratron (P_m), like Edmonds and Hobson (1965) we replace equation (3.2) by the expression:

$$P_c = aP_m(T_c/T_m)^{1/2} \tag{3.3}$$

where a is a factor the value of which is determined by the particular experimental

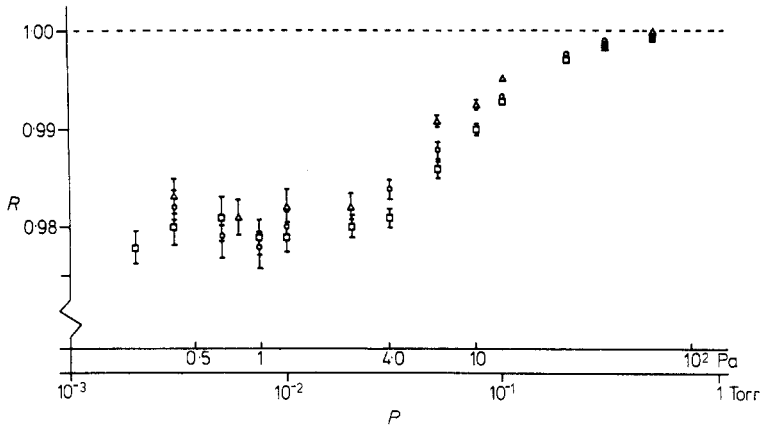

Figure 4. Dependence of the thermal transpiration ratio (R) on the pressure for helium (□), neon (○) and krypton (△).

set-up. From the low pressure limit of $0{\cdot}980 \pm 0{\cdot}002$ we derive a value of $1{\cdot}025 \pm 0{\cdot}002$ for a.

Incorporating equation (3.3) into equation (3.1) finally leads to the following expression for the total cross section:

$$\sigma_{\text{tot}} = -2{\cdot}055(T_c^{1/2}/P_m) \ln[(I_c/I_0)_{\text{gas}}/(I_c/I_0)_{\text{vac}}] \tag{3.4}$$

where σ_{tot} is in a_0^2.

For the derivation of equation (3.4) we adopted the distance between the orifices (42·0 mm) as the absorption length L, but it has to be noted that there is no general agreement about what the effective absorption length actually is. This is due to different assumptions in calculating the density distribution along the axis through the centre of the orifices of the collision chamber for effusive molecular flow patterns (this type of flow always existed in the pressure range of 0·4 to 4 Pa we applied). The effect of the density drop across the orifices can be accounted for by introducing a correction factor α, defined as $L_{\text{eff}} = \alpha L$. A calculation based on the work of Howard (1961) yields a value smaller than unity for α which is confirmed by the calculations of Mathur *et al* (1975) related to geometrical arrangements equal to our collision cell. Both models predict α, the value of which is dependent on the particular gas cell configuration, to be very close to unity for large ratios of L over the orifice diameters. In particular, for the present geometry of the collision chamber we deduce from their work a correction factor between 0·999 and 1·000. Many experimentalists however appear to be supporters of the model of Toburen *et al* (1968). They argue that the density distribution outside the collision chamber remains the same as inside to a distance equal to the radius of the orifice and then falls off as the reverse square of the distance from the orifices. This results in an effective absorption length of $L_{\text{eff}} = L + d_1 + d_2$, where d_1 and d_2 are the diameters of the orifices. None of these models has been sufficiently verified by experiment. Therefore, we changed the collision cell length from 42·0 to 14·2 mm, keeping the orifice diameters constant, and measured the TCS for electron–helium scattering at an impact energy of 60 eV. According to the approach by Mathur *et al* (1975) we had to expect only a slight decrease for the measured cross section (of the order of a few tenths of a per cent). But the approach of Toburen *et al* (1968) predicted an increase of the TCS of the order of 5%. The results of our tests are shown in figure 5.

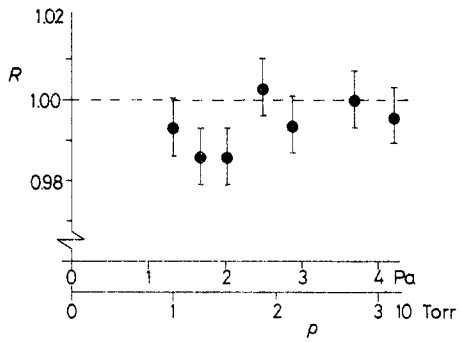

Figure 5. Ratio (R) of the TCS data of 60 eV electrons on He with collision cell length of 14·2 mm and those with length 42·0 mm as a function of the target pressure.

It can be seen that there is perfect agreement with the theory of Mathur *et al* (1975), so we are justified in applying the correction factor $\alpha = 1{\cdot}000$ to the measurements of σ_{tot} at $L = 42{\cdot}0$ mm.

A necessary condition for the reliability of the measurements is the independence of the derived TCS from the target gas pressure and the beam current. Multiple scattering and space charge effects due to ionisation processes in the collision chamber are typically pressure dependent influences on the attenuation of the beam. When carrying out such a test, we have to take care of the transition region for the thermal transpiration ratio R. From figure 4 we see that in the case of helium this region 'sets in' at 4 Pa, whereas for krypton this region has already 'set in' at 1·5 Pa. Below this pressure we can safely use the low pressure limit of R and figure 6(b) shows, for molecular nitrogen, the desired behaviour of the TCS in the range of 0·15 to 1·5 Pa. If space charge effects are present, a dependence on the current may also be expected. However, we did not observe any significant dependence on the current for σ_{tot} in the range of 5×10^{-11} to 10^{-9} A (see figure 6(a)).

A calibration of the electron energy is indispensable since we deal with relatively low energy electrons. This calibration was performed by measuring the position on the energy scale of the pronounced 19·3 eV resonance for electron–helium scattering (see figure 7).

3.2. Error discussion

The only statistical errors of significance are the reading errors of the baratron; these are estimated to give an overall error of 1%.

On the other hand, considering systematical error sources in the derivation of σ_{tot} we are faced with:

(i) the inaccuracy in the measurement of the geometrical absorption length L, which amounts to 0·1%.

(ii) The calibration of the membrane manometer: the manufacturer guarantees an accuracy of 2·0% for a pressure of 0·13 Pa and 0·2% for 1·3 Pa (and so on).

(iii) The linearity of the Keithley 610 A current meter connected with a digital read-out unit: this is better than 0·5%.

(iv) The energy definition: the uncertainty in the energy was estimated to be 0·2 eV (see figure 7); its effect on σ_{tot} depends on the energy and the target gas.

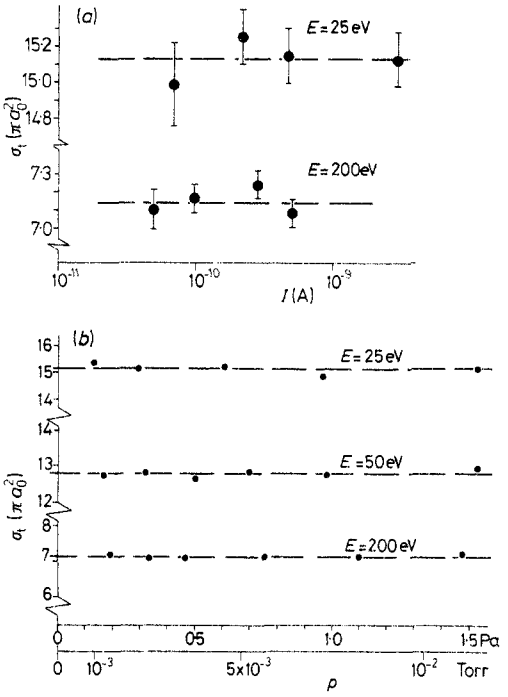

Figure 6. (*a*) Dependence of σ_{tot} on the current for impact energies of 25 and 200 eV. (*b*) Dependence of σ_{tot} on the pressure for impact energies of 25, 50 and 200 eV.

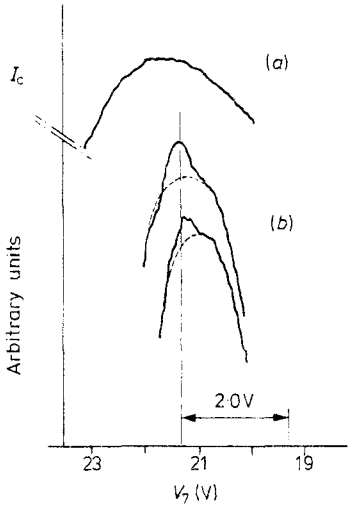

Figure 7. Energy calibration of the primary electron beam by determining the 19·3 eV resonance in helium. As a function of the impact energy (V_7) the analyser signal is displayed in (*a*) without and (*b*) with helium in the gas cell. The energy scale appeared to be shifted over 2 eV (within 0·2 eV accuracy).

The error in the linearity of the current meter propagates via a logarithm in the calculation of the TCS (see equation (3.4)); it is therefore dependent on the attenuation of the beam. In table 3 the errors in the derivation of the TCS for helium and molecular

Table 3. Estimates for the experimental error.

Helium

		Systematical				
E (eV)	Stat.	(*a*)	(*b*)	(*c*)	(*d*)	Total
750	1·0	0·1	0·1	2·0	0·0	3·2
500	1·0	0·1	0·2	2·2	0·0	3·5
200	1·0	0·1	0·2	1·4	0·0	2·7
100	1·0	0·1	0·2	1·4	0·1	2·8
75	1·0	0·1	0·2	1·0	0·2	2·5
50	1·0	0·1	0·2	0·7	0·3	2·3
25	1·0	0·1	0·2	0·7	0·4	2·4
15	1·0	0·1	0·2	0·7	0·5	2·5

Molecular Nitrogen

		Systematical				
E (eV)	Stat.	(*a*)	(*b*)	(*c*)	(*d*)	Total
750	1·0	0·1	1·0	1·8	0·0	3·9
500	1·0	0·1	1·0	1·4	0·0	3·5
200	1·0	0·1	1·0	1·0	0·1	3·2
100	1·0	0·1	1·0	0·7	0·1	2·9
75	1·0	0·1	1·0	0·7	0·1	2·9
50	1·0	0·1	1·0	0·5	0·1	2·7
25	1·0	0·1	1·0	0·5	0·2	2·8
15	1·0	0·1	1·0	0·5	0·3	2·9

(*a*) From the uncertainty of the absorption length.
(*b*) From the uncertainty of the calibration of the manometer.
(*c*) From the uncertainty of the linearity of the current meter.
(*d*) From the uncertainty of the energy definition.
All errors are in per cents.

nitrogen are summarised as a function of the impact energy. In conclusion, we assign to our data a reliability of 4% or better.

4. Discussion of the results

4.1. Electron–helium total cross sections

In table 4 we present the data for σ_{tot} found with our apparatus, together with the experimental and theoretical results obtained by other groups. Our results are interpolated to obtain values at integer values of the energy (the original data set was obtained with smaller intervals, see Blaauw 1979).

First attention will be given to the existing experimental material. For a fuller understanding of the rich collection of data sets, it is worthwhile to make a distinction between the experiments performed with a Ramsauer-type apparatus, i.e. employing a magnetic field perpendicular to the path of the electrons, and those based on quite different techniques. The data of Ramsauer (1921a, b), Brode (1925), Brüche (1927),

Table 4. Total cross sections for electron–helium scattering at low impact energies (data in units of a_0^2)

	Recent experimental					Old experimental						Theoretical		
E (eV)	This work	KB	K	AB	C	RK	N	B	Bru	R	GB	HJ	LC	SN
0				17·20										
1		22·25			21·75	19·66				19·65	19·94		20·77	20·84
2		21·64	21·19	22·20	21·35	21·52	18·57	18·42	19·34	21·04	19·94		20·49	20·84
3		20·64	20·66	22·07	20·75	21·85	17·37	22·00	19·72	21·52	19·30		19·89	20·22
4		19·64	19·96	21·38	20·08	21·26	16·32	22·72	19·38	21·52	18·33		19·20	19·34
5		18·75	19·24	20·35		20·16	15·71	21·25	18·74	21·08	17·44		18·50	18·44
6		18·00	18·54	19·40		18·94	15·41	18·62	17·93	20·43	16·69		17·81	17·64
7		17·25	17·88	18·42		17·85	14·89	16·62	17·32	19·63	15·90		17·14	16·99
8		16·57	17·27	17·58		16·74	14·31	15·10	16·74	18·78	15·08		16·49	16·48
9		15·93	16·44	16·80		16·03	13·73	13·97	16·15	18·06	14·65		15·87	16·05
10		15·36	15·67	16·10		15·29	13·10	13·10	15·57	17·40	13·83		15·28	15·62
11			15·08	15·45		14·82	12·25	12·38	15·06	16·77	13·40			15·13
12		14·14	14·61	14·80		14·37	11·56	11·80	14·57	16·16	12·79			14·53
13			13·95	14·10		13·91	10·97	11·32	14·11	15·54	12·37			13·81
14		13·18	13·52	13·75		13·36	10·50	10·89	13·67	14·93	11·69			13·04
15			12·89	13·20		12·81	10·13	10·50	13·26	14·32	11·33		12·66	12·38
16	12·24	12·25	12·32	12·70		12·32	9·84	10·15	12·87	13·65	10·97			12·09
17	11·76		11·93	12·32		11·88	9·60	9·84	12·49	13·11	10·54			
18	11·57	11·50	11·47	11·90		11·45	9·38	9·58	12·13	12·63	10·22			
19	11·27		11·07	11·55		11·06	9·11	9·31	11·79	12·21	9·58			
20	10·84	10·82	10·71				8·84	9·07	11·46	11·83	9·33		10·62	
21	10·55		10·38				8·58	8·83	11·14	11·49	9·04			
22	10·24	10·21	10·08				8·34	8·61	10·83	11·17	8·69			
23	9·95		9·79				8·11	8·41	10·53	10·87	8·47			
24	9·69	9·68	9·51				7·90	8·21	10·24	10·57	8·26			
25	9·43		9·23				7·70	8·02	9·96	10·27	8·08			
26	9·20	9·18	8·96				7·50	7·84	9·68	9·95	7·89			
27	8·99		8·71				7·32	7·68	9·42	9·62	7·74			
28	8·77	8·71	8·50				7·14	7·52	9·18	9·27	7·65			
29	8·65		8·35				6·97	7·37	8·94	8·99				
30	8·47	8·43					6·80	7·23	8·75	8·73		8·80		

Table 4. (continued). Total cross sections for electron–helium scattering at intermediate and high impact energies (data in units of a_0^2).

	Recent experimental			Old experimental				Theoretical				
E (eV)	This work	KB	JM	N	B	Bru	R	HJ	BW	BJ (EBS)	BJ (OM)	W
32·5	8·03			6·44	6·91	8·24	8·23					
35	7·70	7·64		6·16	6·64	7·83	7·90					
37·5	7·34			6·03	6·50	7·63	7·68					
40	6·97	6·96		5·78	6·20	7·24	7·53	7·27				
42·5	6·77			5·62	6·00	7·00	7·39					
45	6·52	6·46		5·46	5·80	6·78	7·23					
47·5	6·49			5·30	5·63	6·61	7·08					
50	6·17	6·00		5·18	5·50			6·47	7·72			9·61
55	5·81			4·86	5·42							
60	5·46			4·64	5·32			5·70				
65	5·17			4·18	4·99							
70	4·92			4·02	4·83			5·14				
75	4·68			3·93	4·78							
80	4·48			3·89	4·60			4·69				
85	4·34			3·83	4·49							
90	4·20			3·78	4·36			4·40				
95	4·08			3·64	4·23							
100	3·97			3·43	3·94			4·07	5·31	4·68	6·16	6·03
150	3·11		3·22	2·47	3·08			3·15	3·93	3·54		
200	2·58		2·69	2·14	2·63			2·63	3·13	2·92	3·37	3·55
250	2·23											
300	1·98		1·98	1·37	1·90			1·98	2·26	2·15	2·38	2·54
400	1·64		1·61	0·93				1·61	1·79	1·71	1·86	2·00
500	1·35		1·33					1·36	1·49	1·43	1·54	1·67
600	1·19											
700	1·04							1·04	1·12	1·09	1·16	

KB: Kennerly and Bonham (1978)
K: Kauppila *et al* (1977)
AB: Andrick and Bitsch (1975)
C: Crompton *et al* (1970)
RK: Ramsauer and Kollath (1932)
JM: Jost and Möllenkamp (1977)
N: Normand (1930)
B: Brode (1925)
Bru: Brüche (1927)
R: Ramsauer (1921)
GB: Golden and Bandel (1965)
HJ: de Heer and Jansen (1977)
LC: LaBahn and Callaway (1966)
SN: Sinfailam and Nesbet (1972)
BW: Buckley and Walters (1974)
BJ(EBS): Byron and Joachain (1975)
BJ (OM): Byron and Joachain (1977)
W: Winters *et al* (1974).

Normand (1930) and Golden and Bandel (1965) belong to the first category. The data of Ramsauer and Brüche are higher than the present ones, about 5–15% higher for those of Ramsauer and 4–7% higher for those of Brüche, whereas the data of Golden and Bandel are substantially lower. This is striking for the data of Golden and Bandel, since they estimated the error of their data to be about 3%, whereas the difference with the present data is 8–13%. However, a critical reconsideration of the error involved in their pressure determination led Salop and Nakano (1970) to a total error estimation of about 8–10%.

The results of Normand and Brode were obtained with a modified version of the original Ramsauer device (now generally accepted (see Bederson and Kieffer 1971) as

highly unreliable). The data of Brode display a typical behaviour; at 20 eV the difference from our data is about 15%, but for increasing electron energy the difference decreases and becomes less than 5%. In view of the discrepancies of his electron–molecular nitrogen results with our nitrogen data (see next section), we believe this agreement to be fortuitous. The smaller values found by Normand and Brode are by no means surprising; it has already been noticed by Brüche that a large contribution of electrons scattered over small angles is to be expected in their detection cage, especially at high impact energies, thus reducing the measured absorption.

The disagreement with Ramsauer and Brüche is not quite clear. The special shape of the detection cage and its direct location behind the scattering cell in their apparatus may be responsible for substantial back-scattering out of the detector into the scattering cell. In this way they measure too large an absorption.

With regard to the second category of experiments—those using no magnetic field perpendicular to the path of the electrons as energy selector—the situation is more satisfactory. These experiments fall into two classes: those using a differential scattering technique and those using variations on the transmission technique. The Ramsauer–Kollath data (1932) were the the first TCS obtained from absolute differential scattering; the agreement with the present data is good: better than 3%. Andrick and Bitsch (1975) calculated TCS from a phaseshift analysis of their low-energy differential cross section measurements. In the overlapping energy range these data agree with ours within the combined error. Jost and Möllenkamp (1977) obtained TCS in an atomic beam experiment by integration of their angular distribution results for elastic and inelastic scattering separately. Having normalised their results to the absolute measurements of the elastic DCS at small angles of Bromberg (1974) and Jansen *et al* (1976), they claim an overall accuracy of 5% which makes their data fit ours. Very good agreement within 2% is found with the data of Kennerly and Bonham (1978), who employed a time-of-flight method in a linear absorption experiment. From the difference in the time-of-flight spectra with and without gas in the absorption cell they derived the TCS simultaneously for all impact energies below 50 eV. As an overall check of the reliability of their experimental approach for measuring TCS for positrons, Kauppila *et al* (1977) also measured electron–atom scattering cross sections, in the same apparatus. Although no limit on systematical errors has been given, their results can be seen to lie within 3% of ours, with a slight deviation in slope of σ_{tot} as a function of impact energy.

The diffusion experiment of Crompton *et al* (1970, 1977) has yielded momentum transfer cross sections which could be transformed into TCS for low impact energies with high accuracy; the data thus obtained join very well to those of Kennerly and Bonham (1977) and Kauppila *et al* (1977).

Recently de Heer and Jansen (1977) performed semi-empirical calculations of the TCS for electron–helium scattering. These semi-empirical data, based on an analysis of experimental and theoretical TCS data on excitation, ionisation and elastic scattering and of DCS for elastic and inelastic scattering, agree with the present results within the combined error of about 7%.

There have been many calculations of the elastic scattering below the inelastic threshold using a variety of methods. Although our results extend down to only 16 eV, it is still possible to compare them with some of these theoretical data. A good agreement has been found with the polarised orbital calculations of LaBahn and Callaway (1966) and with those of Sinfailam and Nesbet (1972), who introduced a matrix variational method to calculate the low-energy elastic phaseshifts. Moreover

both calculations are also in good agreement with the data of Kennerly and Bonham and of Kauppila *et al.*

The agreement of the present results with the various theoretical calculations at high impact energies (i.e. above 100 eV) is less satisfactory. Comparison is made with the static exchange corrected simplified second Born approximation (SESSBA) calculations of Buckley and Walters (1974), with the second order potential (SOP) calculations of Winters *et al* (1974) and with the eikonal–Born series (EBS) and optical model (OM) calculations of Byron and Joachain (1975, 1977a, 1977b). All these values can be seen to converge only slowly to the present results towards higher energies. At best the deviation is 5% (i.e. for the EBS calculations at 700 eV), but in particular for 100 eV the deviations are considerably larger (up to 58%).

In figure 8 we show the present situation for the TCS for electrons scattered off helium.

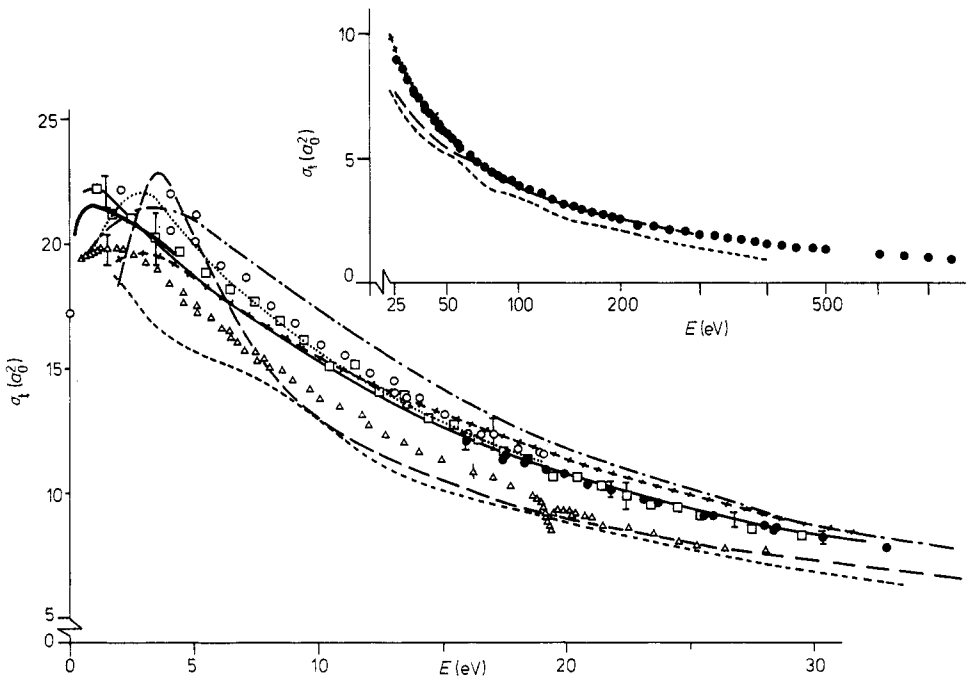

Figure 8. Present situation for the total cross section for electron–helium scattering. ●, this work; ○, Andrick and Bitsch (1975); △, Golden and Bandel (1965); □, Kauppila *et al* (1977); ——, Kennerly and Bonham (1977); ▬▬, Crompton *et al* (1970); · · · ·, Ramsauer and Kollath (1932); × × × ×, Brüche (1927); — · —, Ramsauer (1921); – – – –, Normand (1930); — —, Brode (1925).

4.2. Electron–molecular nitrogen total cross sections

The results are shown in figure 9. Brüche's (1927) data agree within a few per cent with the present ones, better than in the case of helium. The remark by Aberth *et al* (1964) that in their crossed beam recoil experiment electrons can be reflected back into the scattering region causing their data to be 10–20% too high can be considered to be sustained by our measurements. The large deviation from the results of Normand (1930) and Brode (1925) fits in with the observation we made for electron–helium

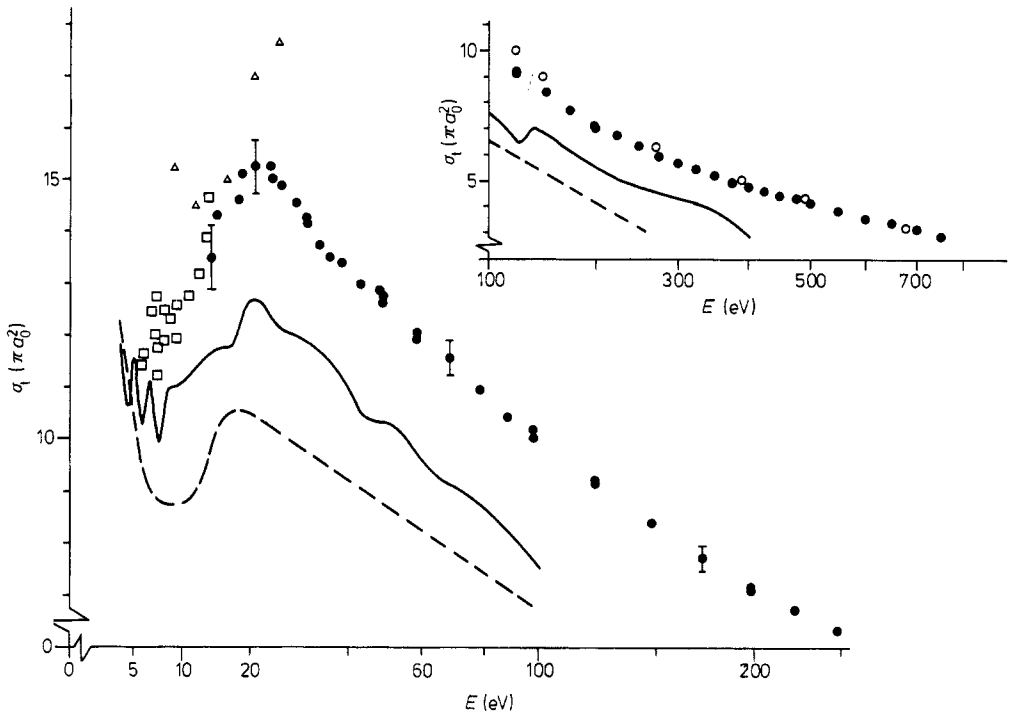

Figure 9. Present situation for the total cross section for electron–molecular nitrogen scattering. ●, this work; □, Brüche (1927); △, Aberth *et al* (1964); ○ Dalba *et al* (1979) (preliminary); ——, Normand (1930); – – –, Brode (1925).

scattering. Very recently A Zecca (1978 private communication) has built an apparatus which resembles that of Golden and Bandel (1965), but with some modifications to make measurements at high impact energies possible. Their preliminary results for N_2 (Dalba *et al* 1979) show an average deviation of 5% from our data.

5. Conclusions

The present apparatus has been shown to be very reliable in producing total cross sections; especially the linearised form made a straightforward determination of the angular resolution possible, thereby overcoming one of the major drawbacks of the former Ramsauer-type designs. The uncertainty in the exact path length, across which the absorption took place, could be removed experimentally. The most recent data from other groups were all, within the combined error range, in perfect accordance with our results. Altogether they map the energy range from 0·3 to 850 eV into a consistent set of TCS data and as a conclusion one might say that the previously existing discrepancies as mentioned in the introduction for helium are herewith resolved.

Acknowledgment

This work is part of the research programme of the Stichting voor Fundamenteel Onderzoek der Materie (Foundation for Fundamental Research on Matter) and was

made possible by financial support from the Nederlandse Organisatie voor Zuiver-Wetenschappelijk Onderzoek (Netherlands Organization for the Advancement of Pure Research).

References

Aberth W, Sunshine G and Bederson B 1964 *Proc. 3rd Int. Conf. on Physics of Electronic and Atomic Collisions* (Amsterdam: North-Holland) Abstracts p 53
Andrick D and Bitsch A 1975 *J. Phys. B: Atom. Molec. Phys.* **8** 393
Baldwin G C and Gaerttner M R 1973 *J. Vac. Sci. Technol.* **10** 215
Bederson B and Kieffer L J 1971 *Rev. Mod. Phys.* **43** 601
Blaauw H J, de Heer F J, Wagenaar R W and Barends D H 1977 *J. Phys. B: Atom. Molec. Phys.* **10** L299
Blaauw H J 1979 *Thesis* FOM Amsterdam
Brode R B 1925 *Phys. Rev.* **25** 636
Bromberg J P 1974 *J. Chem. Phys.* **61** 963
—— 1969 *J. Vac. Sci. Technol.* **6** 801
Brüche E, Lilienthal D and Schrodter K 1927 *Ann. Phys., Lpz.* **84** 279
Buckley B D and Walters H R J 1974 *J. Phys. B: Atom. Molec. Phys.* **7** 1380
Byron F W and Joachain C J 1975 *FOM Report* No 37 p 521
—— 1977a *Phys. Rev.* A **15** 128
—— 1977b *J. Phys. B: Atom. Molec. Phys.* **10** 207
Crompton R W, Elford M T and Jory R L 1967 *Aust. J. Phys.* **20** 369
Crompton R W, Elford M T and Robertson A G 1970 *Aust. J. Phys.* **23** 667
Dalba G, Fornasini P, Lazzizzera I, Ranieri G and Zecca A 1979 *J. Phys. B: Atom. Molec. Phys.* **12** 3787
Edmonds T and Hobson J P 1965 *J. Vac. Sci. Technol.* **2** 192
Gerjuoy E and Krall N A 1960 *Phys. Rev.* **119** 705
—— 1962 *Phys. Rev.* **127** 2105
Golden D E and Bandel H W 1965 *Phys. Rev.* **138** A14
Harting E and Burrows K M 1970 *Rev. Sci. Instrum.* **41** 97
Harting E and Read F H 1976 *Electrostatic Lenses* (Amsterdam: Elsevier)
de Heer F J and Jansen R H J 1977 *J. Phys. B: Atom. Molec. Phys.* **10** 3741
de Heer F J, McDowell M R C and Wagenaar R W 1977 *J. Phys. B: Atom. Molec. Phys.* **10** 1945
de Heer F J, Wagenaar R W, Blaauw H J and Tip A 1976 *J. Phys. B: Atom. Molec. Phys.* **9** L269
Howard W M 1961 *Phys. Fluids* **4** 521
Jansen R H J, de Heer F J, Luyken H J, van Wingerden B and Blaauw H J 1976 *J. Phys. B: Atom. Molec. Phys.* **9** 185
Jost K and Möllenkamp R 1977 *Proc. 10th Int. Conf. on Physics of Electronic and Atomic Collisions* (Paris: Commissariat à l'Energie Atomique) Abstracts p 394
Kauppila W E, Stein T S, Jesion G, Dababneh M S and Pol V 1977 *Rev. Sci. Instrum.* **48** 822
Kennerly R E and Bonham R A 1978 *Phys. Rev.* A **17** 1844
Kessler J and Lindner H 1964 *Z. Angew. Phys.* **18** 7
Knudsen M 1910 *Ann. Phys., Lpz.* **31** 205
LaBahn R W and Callaway J 1966 *Phys. Rev.* **147** 28
Mathur B P, Field J E and Colgate S O 1975 *Phys. Rev.* A **11** 830
Milloy H B and Crompton R W 1977 *Phys. Rev.* A **15** 1847
Normand C E 1930 *Phys. Rev.* **35** 1217
Ramsauer C 1921a *Ann. Phys., Lpz.* **64** 513
—— 1921b *Ann. Phys., Lpz.* **66** 546
Ramsauer C and Kollath R 1932 *Ann. Phys., Lpz.* **12** 529
Salop A and Nakano H H 1970 *Phys. Rev.* A **2** 127
Sinfailam A C and Nesbet R K 1972 *Phys. Rev.* A **6** 2118
Soa E A 1959 *Jenaer Jahrbuch* **1** 115
Stein T S, Kauppila W E, Pol V, Smart J H and Jesion G 1978 *Phys. Rev.* A **17** 1600
Toburen C H, Nakai M Y and Langley R A 1968 *Phys. Rev.* **171** 114
Winters K H, Clark C D, Bransden B H and Coleman J P 1974 *J. Phys. B: Atom. Molec. Phys.* **7** 788